Geochemical Journal, Vol. 51, pp. 251 to 262, 2017 doi:10.2343/geochemj.2.0466

Carbonate ions in high-SiO_2 rhyolite observed in fluid-melt equilibrium experiments

SHUMPEI YOSHIMURA,[1]* MICHIHIKO NAKAMURA[2] and HISAYOSHI YURIMOTO[3,4]

[1]Department of Earth and Planetary Sciences, Hokkaido University, Sapporo 060-0810, Japan
[2]Department of Earth Science, Tohoku University, Sendai 980-8578, Japan
[3]Department of Natural History Sciences, IIL, Hokkaido University, Sapporo 001-0021, Japan
[4]ISAS/JAXA, Sagamihara 252-5210, Japan

(*Received June 27, 2016; Accepted December 27, 2016*)

We carried out equilibrium experiments of the CO_2-H_2O-rhyolite system at 0.1–1.5 GPa and 850 and 1200°C to examine the solubility and speciation of CO_2 in high-SiO_2 rhyolite (SiO_2 > 76 wt%). We observed that both CO_2 molecules (CO_{2mol}) and carbonate anions (CO_3^{2-}) are dissolved in the quenched rhyolitic glasses based on infrared spectroscopy. This result contrasts with the general understanding that high-SiO_2 rhyolitic melt dissolves CO_{2mol} only. The concentrations of CO_{2mol} and CO_3^{2-} were 199–9200 ppm and 58–2100 ppm, respectively, as quantified based on the Beer-Lambert's law and newly determined extinction coefficients of 1192 ± 130 $L \cdot cm^{-1} \cdot mol^{-1}$ and 91 ± 28 $L \cdot cm^{-1} \cdot mol^{-1}$ for CO_{2mol} and CO_3^{2-}, respectively. The water content ranged from 2.6 to 6.1 wt%. Using the thermodynamic analysis, we calculated the partial molar volume of CO_{2mol} to be $\overline{V}^{melt}_{CO2mol}$ = 24.9 ± 2.0 cm^3/mol and enthalpy of dissolution to be $\Delta_{sln}H$ = –22.2 ± 6.3 kJ/mol. Changes in volume and enthalpy upon the formation reaction of CO_3^{2-} were calculated to be $\Delta_r V$ = –8.6 ± 0.9 cm^3/mol and $\Delta_r H$ = +1.1 ± 4.4 kJ/mol, respectively.

Keywords: rhyolite, CO_2, solubility, species

INTRODUCTION

Carbon dioxide is a major volatile component in the Earth, and it controls igneous processes and volcanic activity by changing the physicochemical properties of magma. Rhyolitic magma may contain significant concentration of CO_2 and, thus, plays a crucial role in the CO_2 transfer within the crust, as suggested by analyses of volcanic glass (e.g., Wallace *et al*., 1999; Anderson *et al*., 2000; Rust *et al*., 2004; Bachmann *et al*., 2009; Blundy *et al*., 2010) and volcanic gases (e.g., Harris *et al*., 1981; Harris and Rose, 1996). In order to understand the behaviour of CO_2 in the crustal magma, the CO_2 solubility in rhyolitic melt is of fundamental importance.

Previous experimental studies have revealed the basic characteristics of the solubility and speciation of CO_2 in rhyolitic melts. In 'high-SiO_2' rhyolitic melt (SiO_2 > ~76 wt%), it was considered that CO_2 dissolves solely as CO_2 molecules (CO_{2mol}). Its solubility is linearly proportional to the CO_2 fugacity at below ca. 0.5 GPa, while the solubility behaves non-ideally at above 0.5 GPa (Blank, 1993; Blank *et al*., 1993; Fogel and Rutherford, 1990; Tamic *et al*., 2001). For 'low-SiO_2' rhyolitic melts (rhyodacitic composition; SiO_2 = 68~74 wt%), both CO_{2mol} and CO_3^{2-} coexist (Brooker *et al*., 1999; Duncan and Dasgupta, 2014, 2015), which is similar to melt with intermediate compositions (Mysen *et al*., 1975; Mysen, 1976; Brey, 1976; Fine and Stolper, 1985; Stolper *et al*., 1987; Brooker *et al*., 1999; King and Holloway, 2002; Morizet *et al*., 2002; Behrens *et al*., 2004a; Nowak *et al*., 2004; Botcharnikov *et al*., 2005, 2006). Currently, solubility data for high-SiO_2 rhyolite under pressures higher than 0.66 GPa are lacking. Although recent solubility models have predicted the CO_2-H_2O solubility under high-pressure conditions (e.g., Papale *et al*., 2006; Duan, 2014; Ghiorso and Gualda, 2015), additional experimental data are necessary to examine validity of these models. In addition, the possibility that CO_3^{2-} may be present in high-SiO_2 rhyolite (Moore *et al*., 2008) is still controversial and needs re-examination.

In this paper, we present new experimental results of CO_2-H_2O solubility in a high-SiO_2 rhyolitic melt (SiO_2 = 77.8 wt%) at 850 and 1200°C and at 0.1–1.5 GPa. We then discuss the solubility and speciation of the experimental products.

*Corresponding author (e-mail: shumpyos@sci.hokudai.ac.jp)

Table 1. Chemical compositions of starting material

Oxides	wt% [a]
SiO_2	77.81
TiO_2	0.14
Al_2O_3	12.65
FeO^t [b]	0.52
MnO	0.05
MgO	0.05
CaO	0.40
Na_2O	3.06
K_2O	4.65
H_2O [c]	0.66
CO_2	0.00
Total [d]	100.00

[a]*Data from Yoshimura and Nakamura (2010).*
[b]*Total Fe as FeO.*
[c]*Measured by FT-IR analysis.*
[d]*Normalised to 100%.*

EXPERIMENTAL AND ANALYTICAL PROCEDURE

Experiments were carried out using either a piston-cylinder apparatus or a cold-seal pressure vessel at Tohoku University. The starting material for the rhyolitic melt was unaltered, transparent rhyolitic obsidian obtained from a working quarry in Wada-Pass, central Japan. The major and volatile compositions of this obsidian are given in Table 1. The experimental conditions are summarised in Table 2.

Piston cylinder experiments and volatile analyses

For the piston-cylinder experiments, obsidian flakes (thinner than 1 mm) and oxalic acid dihydrate ($(COOH)_2{\cdot}2H_2O$) were put in a 5-mm-diameter, 12-mm-long platinum-sleeved nickel capsule. The capsule was capped with a platinum gasket and a nickel lid, and placed in an NaCl-Pyrex assembly (Fig. 1). The assembly was cold pressurised to about 80% of the desired pressure. An electrical current was then switched on to heat the sample under programmed control. When the temperature reached 1200°C, the pressure was carefully increased until the final desired value was attained. No frictional correction on pressure was made in this study. All piston-cylinder experiments were performed for 3 hours. The oxygen fugacity (f_{O2}) within the capsule is considered to be close to that buffered by Ni-NiO, as was investigated for the cell assembly having the similar design (Brenan and Watson, 1988; Watson and Lupulescu, 1993; Lupulescu and Watson, 1999; Nakamura and Watson, 2001). The equilibrium calculation based on the CEA programme (Gordon and McBride, 1996) showed that under this f_{O2} condition at 1200°C and 1 GPa, the dominant spe-

Table 2. Experimental conditions and results

Run# [a]	T	P	t	X_{CO2}^{fluid}	CO_{2bulk} [b]	CO_{2mol}	CO_3^{2-}	CO_{2tot}	CO_3^{2-}/CO_{2tot}	H_2O_{mol}	OH	H_2O_{tot}
	[°C]	[GPa]	[h]		[ppm]	[ppm]	[ppm]	[ppm]		[wt%]	[wt%]	
c21	850	0.10	96	0.25[c]	n.d.	199 (22)[d]	58 (26)[d]	257 (34)[d]	0.225 (0.104)[d]	2.04 (0.10)[d]	1.63 (0.14)[d]	3.67 (0.24)[d]
c04	850	0.20	96	0.52[c]	n.d.	711 (78)	72 (46)	782 (91)	0.092 (0.060)	2.13 (0.11)	1.59 (0.14)	3.72 (0.25)
p54	1200	0.50	3	0.79	n.d.	1943 (281)	232 (101)	2175 (298)	0.107 (0.049)	0.53 (0.09)	2.08 (0.39)	2.61 (0.48)
p59	1200	0.77	3	0.76	4145	3776 (437)	568 (176)	4343 (471)	0.131 (0.043)	2.70 (0.16)	1.85 (0.17)	4.55 (0.33)
p66	1200	1.49	3	0.78	12111	9188 (1143)	2123 (654)	11312 (1317)	0.188 (0.062)	4.12 (0.24)	1.97 (0.25)	6.09 (0.49)

[a]*"c" represents cold-seal experiments, and "p" represents piston cylinder experiments.*
[b]*Measured by the vacuum extraction method.*
[c]*Estimated from concentrations of CO_{2mol} and H_2O_{tot} and solublity law of Liu et al. (2005).*
[d]*Parentheses indicate 1σ standard deviation.*

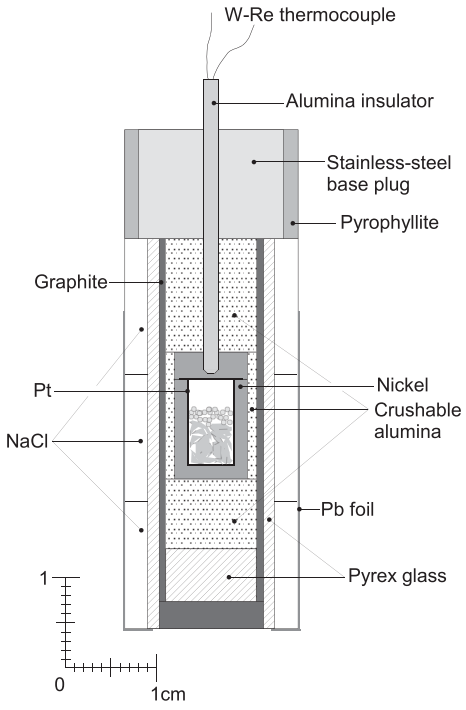

Fig. 1. A schematic illustration of the NaCl-Pyrex cell for piston-cylinder experiments.

cies in the fluid are CO_2 and H_2O. After each run, the sample was quenched by turning off the heater. The quench rate was 60–40°C/s from 1200 to 580°C and 40–20°C/s to 300°C.

The composition of the coexisting fluid in the capsule was analysed using a cryogenic method. First, the thick nickel lid was removed from the platinum gasket by hand. In successful experiments, the platinum gasket was domically inflated, indicating that the experiment was fluid supersaturated. The capsule was then cleaned ultrasonically in acetone and loaded into a glass tube connected to a vacuum extraction line. After evacuating the air, the capsule was pierced with a stainless steel nail; the gas that burst from the nail hole was captured in a liquid nitrogen trap. When the run duration was longer than 3 hours, the lid was so tightly welded to the capsule that the fluid analysis was not possible. The capsule was gently heated with a heat gun for 10–20 minutes to promote degassing from the capsule. The trapped gas was separated into pure CO_2 and H_2O using liquid nitrogen and a dry ice-ethanol slurry. The amount of the CO_2 gas (n_{CO2}^{fluid} (mol)) was quantified based on manometry in a calibrated volume. The pressure of the gas was measured using an Ulvac G-TRAN CCMT-100D ceramic capacitance manometer. Accuracy of the pressure measurement was within 0.4%, which corresponds to $<3.8 \times 10^{-7}$ mol CO_2 in our manometry line. After analysing CO_2, the amount of H_2O (n_{H2O}^{fluid} (mol)) was measured in the same manner. The fluid composition was defined as the molar fraction of CO_2:

$$X_{CO_2}^{fluid} = \frac{n_{CO_2}^{fluid}}{n_{CO_2}^{fluid} + n_{H_2O}^{fluid}}. \quad (1)$$

After fluid analysis, the rhyolitic glass was recovered from the capsule. Glass samples in successful runs were colourless and transparent; these samples were doubly polished to 60–71 μm thick wafers and analysed with a Jasco FTIR-6100 equipped with IRT-3000N microscope. These thicknesses were selected such that absorbances of less than 1.8 could be obtained, because if absorbance exceeds 1.8, slight variations in the thickness of the wafer and non-linearity in the detector response can lead to large errors (Ihinger *et al.*, 1994). Some glass contained a small number of tiny bubbles (<0.1% in volume and <5 μm in diameter, respectively). Such bubbles were carefully avoided in IR-spectroscopic analyses. For CO_2 concentrations, a peak height of 2280 cm^{-1} ($^{13}CO_{2mol}$) or 2350 cm^{-1} ($^{12}CO_{2mol}$) for CO_2 molecules and 1410 cm^{-1} for carbonate anions, was measured respectively. As shown in Subsection "Concentration and speciation of CO_2", both CO_{2mol} and CO_3^{2-} were observed in our glass samples: the concentrations of each species were quantified based on the Beer-Lambert's law and the absorption coefficients newly determined in this study. To quantify the absorbance of the 1410 cm^{-1} peak, we used the background-subtraction method. We first subtracted the infrared spectrum of the starting obsidian from the spectrum of carbonated samples, and then measured the absorbance from a linear base line that passes two local minima near the peak or one local minimum and a point at which the gradient is the lowest. Concentrations of H_2O molecules (H_2O_{mol}) and hydroxyl groups (OH) in the glass were determined from the peak height of 5250 cm^{-1} (H_2O_{mol}) and 4500 cm^{-1} (H_2O_{mol}) and extinction coefficients reported in Okumura and Nakashima (2005) (1.75 ± 0.08 $L \cdot cm^{-1} \cdot mol^{-1}$ for the 5250 cm^{-1} peak and 1.42 ± 0.12 $L \cdot cm^{-1} \cdot mol^{-1}$ for the 4500 cm^{-1} peak).

In some experiments, the bulk analysis of total dissolved CO_2 in the glass was carried out using a vacuum extraction line. Glass fragments measuring a few ten mg were taken from the capsule and loaded in a quartz glass reaction vessel. This vessel had been pre-heated at 1000°C for more than 6 h and stored in a vacuum desiccator before use. After evacuation, the sample was heated at 1200°C for 1 h to degas completely. The gas obtained was collected in a liquid nitrogen trap, purified cryogenically, and analysed manometrically in the same manner as the fluid analysis. We analysed only CO_2, and H_2O was not quantified.

Cold-seal experiments

Two sets of lower pressure experiments (c21 and c04) were carried out using a cold-seal pressure vessel. The experimental procedure was identical to that of Yoshimura and Nakamura (2010). An obsidian slab, oxalic acid dihydrate, and Ni-NiO powder were put in a gold tube, and the capsule was arc-welded shut. The capsule was then put in a René 41 reactor and run at 0.1 and 0.2 GPa and 850°C for 96 h. The vessel was isobarically quenched by blowing compressed air for 10 min. After quenching, the glass was recovered from the capsule, doubly polished to 215 and 228 μm thick wafers and analysed by IR spectroscopy. The capsule made a hissing sound when it was pierced with an iron needle, showing fluid supersaturation. Unfortunately, the composition of the coexisting fluid was not determined experimentally. Therefore, X_{CO2}^{fluid} in the cold-seal experiments was estimated by comparing the H_2O and CO_2 content of the glass with the solubility law derived by Liu *et al*. (2005).

Experimental Results

Concentration and speciation of CO_2

The experimental results are summarised in Table 2—a full set of results including absorbance of each peak in infrared spectroscopy and wafer thicknesses is provided in Supplementary Table S1. Figure 2a shows a typical IR spectrum of recovered rhyolitic glass, showing the presence of H_2O and CO_2. An important finding in this study is that a peak exists at 1410 cm^{-1} in all the samples (Fig. 2b). This peak corresponds to the v_3 asymmetric stretching motion of carbonate anions (CO_3^{2-}) (e.g., Blank and Brooker, 1994), indicating that CO_3^{2-} is present in our rhyolitic glass.

For quantification of concentrations of CO_{2mol} and CO_3^{2-}, we newly determined extinction coefficients of 2350 cm^{-1} and 1410 cm^{-1}. The total CO_2 content measured by bulk analysis ($C_{CO2bulk}$) is the sum of the CO_3^{2-} and CO_{2mol} contents. This relation is described based on Beer-Lambert's law as:

$$C_{CO_{2bulk}} = \frac{M_{CO_2} Abs_{2350}}{\rho d \varepsilon_{2350}} + \frac{M_{CO_2} Abs_{1410}}{\rho d \varepsilon_{1410}} \qquad (2)$$

where Abs_{2350} is the absorbance of 2350 cm^{-1} (CO_{2mol}), Abs_{1410} is the absorbance of 1410 cm^{-1} (CO_3^{2-}), d is the thickness of glass wafer (cm), M_{CO2} is the molar mass of CO_2 (44.01 g·mol^{-1}), ε_{2350} is the extinction coefficient of 2350 cm^{-1}, ε_{1410} is the extinction coefficient of 1410 cm^{-1}, and ρ is glass density (kg/m^3). ρ was calculated as a function of the water content: $\rho = \rho_0 - m \times C_{H2Otot}$, where C_{H2Otot} is the total H_2O content in wt%, m is a constant (14 kg/(m^3·wt%)) and ρ_0 is density of anhydrous glass (2352 kg/m^3) (Okumura and Nakashima, 2005). Fitting Eq. (2) to the data of p59, p66 and an early exploratory experiment ($C_{CO2bulk}$ = 8611 ± 245 ppm, Abs_{2280} = 0.0376 ± 0.0031, Abs_{1410} = 0.1592 ± 0.0849 and ρ = 2284

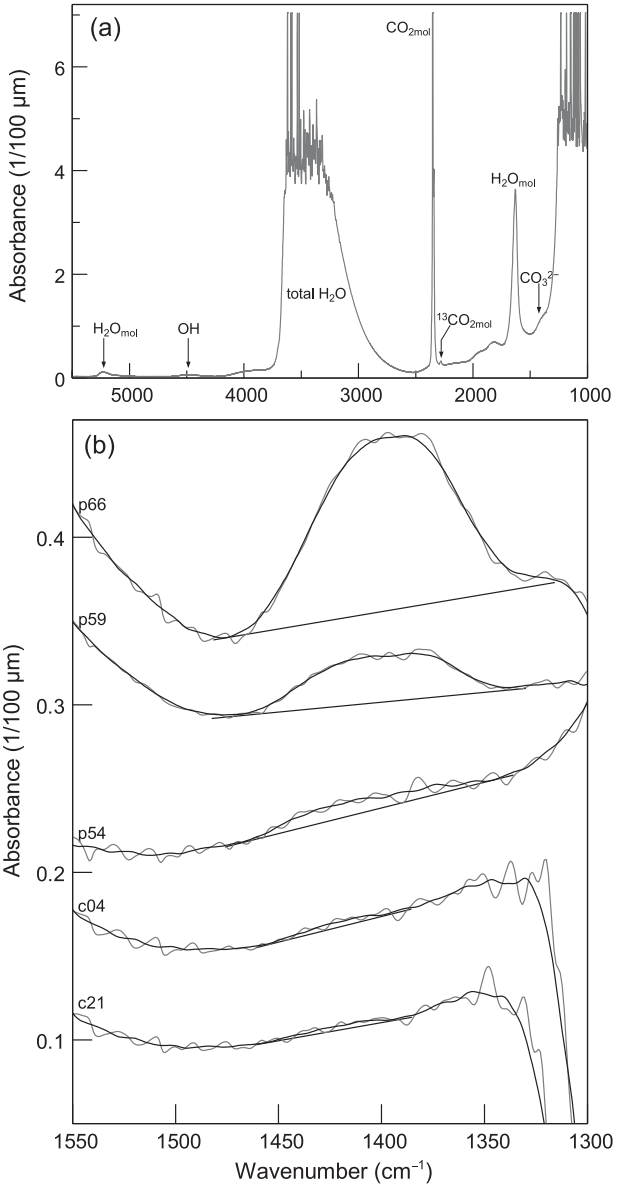

Fig. 2. (a) Typical IR spectrum of our experimental rhyolitic glass (run# p66). Peaks are observed at 1410 cm^{-1} (carbonate anions; CO_3^{2-}), 1630 cm^{-1} (H_2O molecules; H_2O_{mol}), 2280 cm^{-1} ($^{13}CO_2$ molecules), 2350 cm^{-1} ($^{12}CO_2$ molecules; CO_{2mol}), 3550 cm^{-1} (total H_2O), 4500 cm^{-1} (hydroxyl groups, OH), and 5250 cm^{-1} (H_2O_{mol}). Spectra were normalised to wafer thickness of 100 μm. (b) Background-subtracted spectra of the experimental glasses, produced by subtracting the spectrum of CO_2-free glass (starting obsidian) from each spectrum of experimental samples. Grey and black lines indicate original and smoothed (moving point averaged) spectra, respectively.

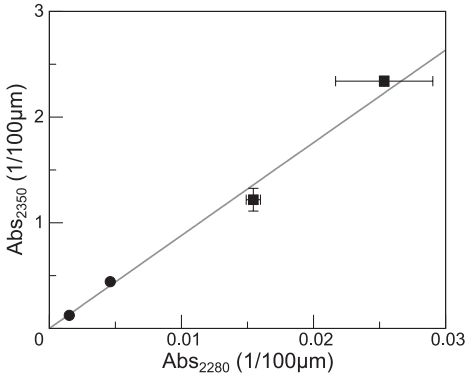

Fig. 3. Linear relation between absorbance of the peaks at 2350 cm^{-1} ($^{12}CO_{2mol}$) and 2280 cm^{-1} ($^{13}CO_{2mol}$) ($Abs_{2350} = (87.6 \pm 3.1) \times Abs_{2280}$), as obtained from runs c21, c04, p54, and p59. This relation was used to estimate the CO_{2mol} content of run p66.

± 12 kg/m^3), we determined ε_{2350} and ε_{1410} to be 1192 ± 130 L·cm^{-1}·mol^{-1} and 91 ± 28 L·cm^{-1}·mol^{-1}, respectively.

For the highest pressure sample (p66), it was impossible to quantify the absorbance of 2350 cm^{-1}, because the molecular CO_2 content was so high that the 2350 cm^{-1} peak height was not accurately quantified even in a sample that was 71 μm thick. In this case, we measured the absorbance of 2280 cm^{-1} (Abs_{2280}), which represents $^{13}CO_2$ molecules, and converted Abs_{2280} to Abs_{2350} using a linear relation, $Abs_{2350} = (87.6 \pm 3.1) \times Abs_{2280}$ (Fig. 3). This equation was obtained by fitting a linear equation to the data set of c21, c04, p54 and p59. The linearity holds as long as the carbon isotope ratio does not change so much.

Figure 4a shows concentrations of CO_{2mol} and CO_3^{2-} as a function of the total CO_2 (CO_{2tot}) content. Both CO_{2mol} and CO_3^{2-} contents increased with increasing the total CO_2 content. The fraction of CO_3^{2-} to total CO_2 generally increased with an increase in total CO_2 (Fig. 4b). The run with the lowest CO_{2tot} content (c21) was accompanied by large errors because the CO_3^{2-} content was below the detection limit, and was therefore not used in thermodynamic calculations of Subsection "Thermodynamics of CO_{2mol} and CO_3^{2-} speciation and solubilities for rhyolitic melt".

In all experiments, CO_2 and H_2O concentrations were spatially homogeneous within error in multiple point analysis of a *ca.* 1 mm × 2 mm glass wafer.

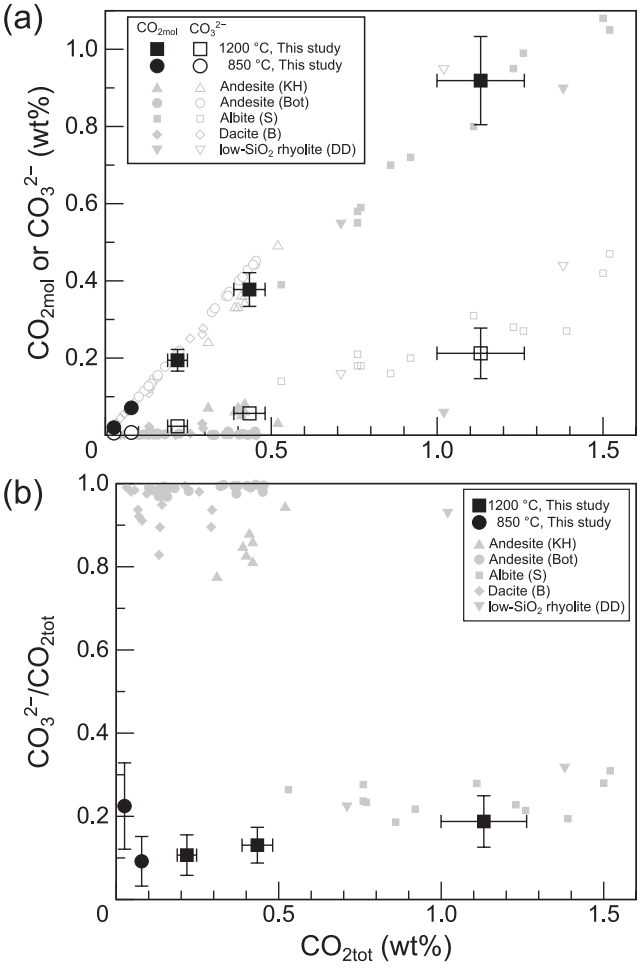

Fig. 4. (a) Concentrations of CO_{2mol} and CO_3^{2-} in rhyolitic glass as a function of total CO_2 content. Black squares: 1200 °C experiments; Black circles: 850 °C experiments. Solid symbols represent CO_{2mol} and open symbols represent CO_3^{2-}. Grey symbols represent data from previous studies, including albite melt (squares: 1.5–3 GPa, 1450–1625 °C, Stolper et al., 1987 (S)), andesite melt (triangles: King and Holloway, 2002 (KH); circles: Botcharnikov et al., 2006 (Bot)), dacite melt (diamonds: Behrens et al., 2004a (B)) and low-SiO_2 rhyolite (upside-down triangles: Duncan and Dasgupta, 2015 (DD)). (b) Fraction of CO_3^{2-} as a function of total CO_2 content. Run c21 (at 0.1 GPa) was accompanied by large error due to an insufficient content of CO_3^{2-}, and was not used in the thermodynamic calculations in Subsection "Thermodynamics of CO_{2mol} and CO_3^{2-} speciation and solubilities for rhyolitic melt". Note that the CO_{2mol} content is higher than the CO_3^{2-} content for rhyolitic and albite melts while it is opposite for dacite and andesite melts.

Concentration and speciation of H_2O

Figure 5 shows the concentrations of H_2O molecules (H_2O_{mol}) and OH in the rhyolitic melt as a function of the H_2O_{tot} content. The H_2O_{tot} content ranged 2.6–6.1 wt%. The H_2O_{mol} concentration was higher than OH concentration in all experiments, except for run p54, in which the OH content was higher than the H_2O_{mol} content. As discussed in Subsection "Speciation of H_2O", such a difference in H_2O speciation reflects the difference in cooling history during quenching.

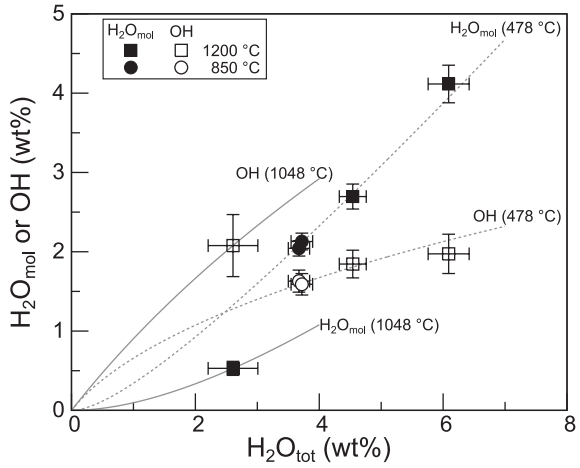

Fig. 5. Concentrations of OH and H_2O_{mol} in rhyolitic melt as a function of total H_2O (H_2O_{tot}) content. Squares: 1200°C experiments; circles: 850°C experiments. Solid and open symbols represent H_2O_{mol} and OH, respectively. The apparent equilibrium temperature of the H_2O dissociation reaction was calculated to be 1048 and 478 ± 19°C for run p54 and other runs, respectively (Ihinger et al., 1999). Grey solid and broken lines indicate equilibrium speciation in the H_2O dissociation reaction at 1048 and 478°C, respectively.

Fluid composition

For the piston-cylinder experiments, the fluid composition determined using manometry was X_{CO2}^{fluid} = 0.76–0.79. In the cold-seal experiments, X_{CO2}^{fluid} was estimated as 0.25 and 0.52 for runs c21 and c04, respectively, based on the CO_{2mol} and H_2O_{tot} contents of the quenched glass and the solubility law of Liu *et al*. (2005). The total saturation pressures were calculated to be 0.12 GPa for run c21 and 0.22 GPa for run c04, which were slightly higher than the actual experimental pressures of 0.10 GPa and 0.20 GPa. When the solubility model by Ghiorso and Gualda (2015) and the CO_{2tot} and H_2O_{tot} contents were used, X_{CO2}^{fluid} for runs c21 and c04 were calculated to be 0.2 and 0.4, respectively (Fig. 6a). When the solubility model by Duan (2014) was used, X_{CO2}^{fluid} for runs c21 and c04 were calculated to be 0.3 and 0.6, respectively (Fig. 6b). In this study, we used values obtained by the model of Liu *et al*. (2005) for thermodynamic calculations in Subsection "Thermodynamics of CO_{2mol} and CO_3^{2-} speciation and solubilities for rhyolitic melt", considering that X_{CO2}^{fluid} values by Liu *et al*. (2005) are the intermediate values between values by Duan (2014) and Ghiorso and Gualda (2015).

Volatile loss in the piston-cylinder experiments

The fluid composition in the piston-cylinder experiments, X_{CO2}^{fluid} = 0.76–0.79, is much richer in CO_2 than what was expected from the simple decomposition of oxalic acid dihydrate under f_{O2} controlled by the Ni-NiO equilibrium reaction (X_{CO2}^{fluid} = 0.4). Such CO_2-rich fluids are generated when the mass ratio of fluid to melt in the capsule is low. A mass-balance calculation showed that the mass ratio of fluid to melt, before the run, was 0.20–0.24; however, this value decreased to 0.06–0.17 after the run, indicating that a part of the fluid leaked during the experiment. The most likely explanation for this volatile loss is the delayed sealing of the capsule. In the present experiments, the capsule was not arc-welded, because a stable temperature control could not be maintained in our piston-cylinder system when a capsule with both ends arc-welded was used. Instead, the Pt gasket was cold pressurised to the sealing plane (the upper part of the ashtray-shaped Pt sleeve; Fig. 1). Therefore, both a selective loss of H_2O vapour at an initial stage of the heating by a dehydration reaction $(COOH)\cdot 2H_2O \rightarrow (COOH)_2 + 2H_2O$ or loss of H_2O-CO_2 mixture after decomposition of $(COOH)_2$ may have occurred prior to platinum welding. In the early stages of this study, we often suffered more significant fluid loss, and many experiments were discarded. After discovering that the sealing plane had micro-scale roughness that might have allowed a part of fluid leak to the outside before the Pt sintering was completed, we carefully polished the Pt sealing planes to a mirror finish. As a result, the volatile loss was drastically mitigated, and we used this method for all the runs presented in this paper. Considering that the rate of Pt sintering is controlled by metal self-diffusion (Kingery and Berg, 1955), we assume that the Pt sintering was complete during the last a few minutes of the initial heating to 1200°C, and no significant volatile loss occurred during the period of the fluid-melt equilibrium.

Discussion

Comparison of ε_{2350} and ε_{1410} with previous data

We determined ε_{2350} (CO_{2mol}) to be 1192 ± 130 $L\cdot cm^{-1}\cdot mol^{-1}$ and ε_{1410} (CO_3^{2-}) to be 91 ± 28 $L\cdot cm^{-1}\cdot mol^{-1}$. This ε_{2350} is similar to that of Behrens *et al*. (2004b) (1214 ± 78 $L\cdot cm^{-1}\cdot mol^{-1}$) and Duncan and Dasgupta (2015) (1227 ± 108 $L\cdot cm^{-1}\cdot mol^{-1}$), and slightly higher than that of Blank (1993) (1066 ± 20 $L\cdot cm^{-1}\cdot mol^{-1}$). For ε_{1410}, our value is smaller than that of Duncan and Dasgupta (2015) (143 ± 10 $L\cdot cm^{-1}\cdot mol^{-1}$) which was reported for low-SiO_2 rhyolitic glass (SiO_2 = 68 wt%). Brooker *et al*. (1999) showed that the ε_{1410} (ε_{1350}) of $NaAlO_2$-SiO_2 melts decreases with increasing the SiO_2 content, from 360 $L\cdot cm^{-1}\cdot mol^{-1}$ for nepheline glass to 145 $L\cdot cm^{-1}\cdot mol^{-1}$ for an 'Eu' (eutectic composition) glass. The value produced by our study is consistent with the trend that ε_{1410} decreases with increasing SiO_2 content (Fig. 7).

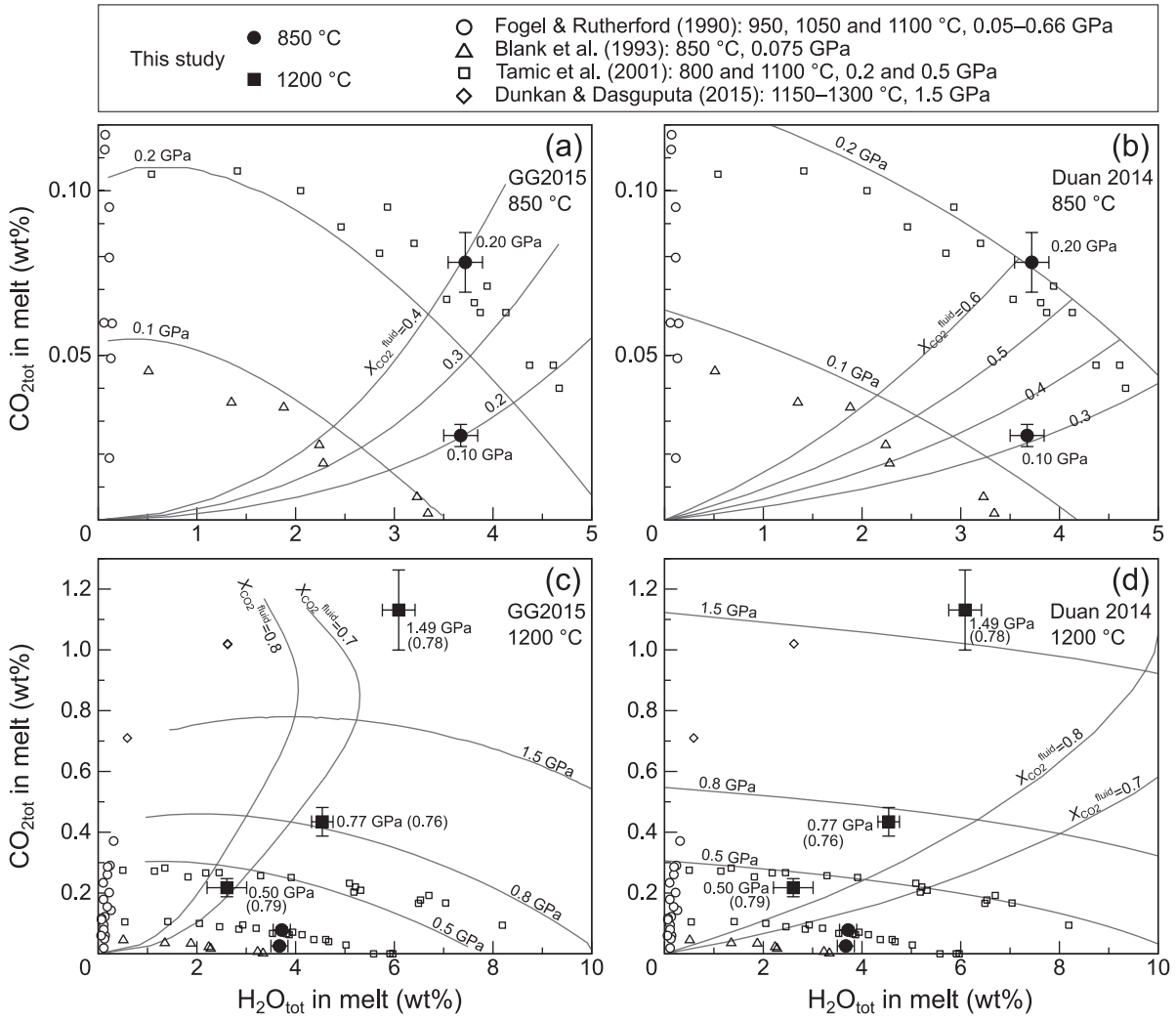

Fig. 6. H_2O_{tot}-CO_{2tot} diagrams comparing our experimental results with solubility models of Duan (2014) and Ghiorso and Gualda (2015) ('GG2015'); results from previous studies on rhyolite are also plotted (Fogel and Rutherford, 1990; Blank et al., 1993; Tamic et al., 2001; Dunkan and Dasgupta, 2015). Isobars and isopleth are drawn based on the models by (a, c) Ghiorso and Gualda (2015) and (b, d) Duan (2014). Temperatures are (a, b) 850°C, and (c, d) 1200°C. The rhyolite composition listed in Table 1 was used to obtain the solubility curves. Values on isobars represent the total pressure, and values on isopleths represent X_{CO2}^{fluid}. Experimental pressures (and X_{CO2}^{fluid} in parentheses in c and d) are indicated next to the plotted points.

Comparison of CO_2-H_2O solubility with previous solubility models

Figures 6c and d represent the H_2O-CO_2 diagram for 1200°C comparing our high-pressure experimental results with previous experimental data for rhyolite (Fogel and Rutherford, 1990; Blank *et al*., 1993; Tamic *et al*., 2001; Duncan and Dasgupta, 2014) and the two latest solubility models (Duan, 2014; Ghiorso and Gualda, 2015). Figure 6c shows that our solubility result at 0.77 GPa is roughly consistent with the 0.8 GPa isobar of Ghiorso and Gualda (2015), while for other pressures, our results were not well reproduced by this model: at 1.5 GPa our solubility was much higher than the 1.5 GPa isobar, and at 0.5 GPa, our solubility was slightly lower than the 0.5 GPa isobar. In addition, our results showed much H_2O-richer solubilities than expected from the isopleth of Ghiorso and Gualda (2015) and the observed X_{CO2}^{fluid} (=0.7–0.8).

Figure 6d represents a comparison with the solubility model by Duan (2014). The H_2O-CO_2 concentrations obtained in our experiments are better reproduced by the Duan's isobars within error for all piston cylinder runs. However, our results showed much CO_2-richer solubilities than predicted from the isopleths of X_{CO2}^{fluid} = 0.8–0.7. For cold-seal experiments, our solubility at 0.2 GPa was well reproduced by the Duan's isobar, while the 0.1 GPa

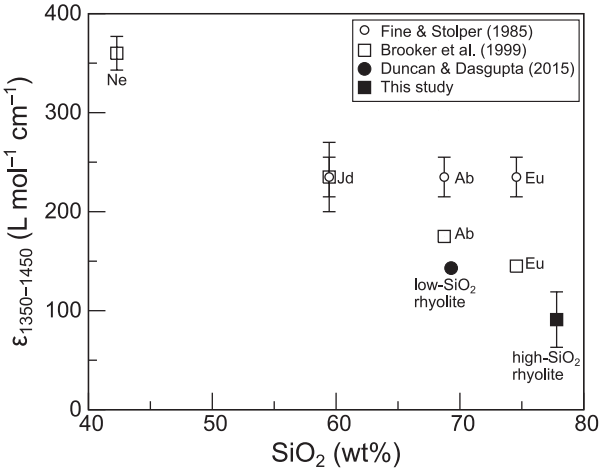

Fig. 7. Extinction coefficient of a peak at 1350–1430 cm^{-1} (CO_3^{2-}) as a function of the SiO_2 content. The symbols denote the following: ■, this study; ○, Fine and Stolper (1985); □, Brooker et al. (1999); ●, Duncan and Dasgupta (2015). Ab: the albite composition ($NaAlSi_3O_8$); Eu: the composition close to that of the 1-atm albite-quartz eutectic point ($NaAlSi_4O_{10}$); Jd: the jadeite composition ($NaAlSi_2O_6$); Ne: the nepheline composition ($NaAlSiO_4$). Note that the data from Fine and Stolper (1985) were obtained as a single value (235 ± 20 L mol^{-1} cm^{-1}) on an assumption that the molar absorptivity has no compositional dependence between Jd and Eu melts.

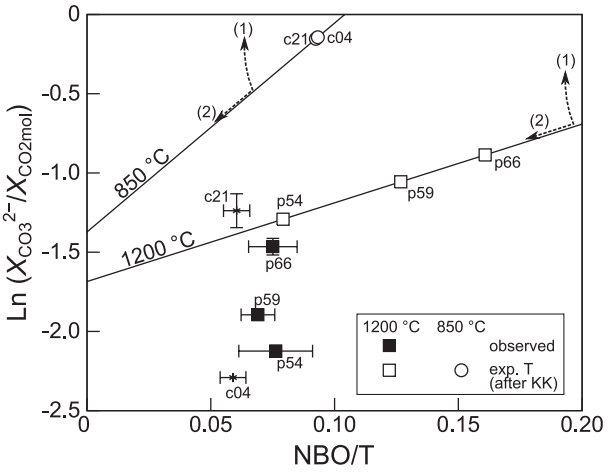

Fig. 8. CO_3^{2-}/CO_{2mol} ratios and NBO/T values observed in quenched glass samples and those estimated for high temperature melts. The NBO/T values were calculated based on Zotov et al. (1992), according to the assumption that OH serves as a network modifier while H_2O_{mol} does not. For estimation of the NBO/T values at experimental temperatures, we calculated the OH concentration before re-equilibration (Reaction (3)) based on the model of Ihinger et al. (1999), and used it to calculate the NBO/T values. Equilibrium CO_3^{2-}/CO_{2mol} ratios were estimated using the model proposed by Konschak and Keppler (2014): $In(X_{CO32-})/X_{CO2} = a + b/T$, where $a = -2.69 - 21.38 \times (NBO/T)$, $b = 1480 + 38810 \times (NBO/T)$, and T is temperature in Kelvin. Arrow (1) indicates the increase in the CO_3^{2-}/CO_{2mol} ratio and the slight decrease in the NBO/T value as a result of low-temperature re-equilibration (the reaction (4) shifts to the right). Arrow (2) indicates the decrease in the CO_3^{2-}/CO_{2mol} ratio as a result of the decrease in NBO/T values caused by H_2O re-equilibration at low temperatures.

experiment showed slightly higher CO_2-H_2O concentrations than the 0.1 GPa isobar. In conclusion, we consider that Duan's (2014) solubility is presently the most successful at predicting solubility under low to high pressures for high-SiO_2 rhyolite, although the isopleths are still inconsistent with the experimental results.

Speciation of H_2O

It is well known that H_2O dissolves as OH and H_2O_{mol} in the melt through the following reaction (e.g., Silver and Stolper, 1989):

$$H_2O_{mol}\ (melt) + O\ (melt) \leftrightarrow 2OH\ (melt) \qquad (3)$$

where O denotes an anhydrous oxygen (bridging oxygen) (Zhang, 1999). This reaction shifts to the left at low temperatures, leading to a decrease in the OH/H_2O_{mol} ratio. Based on the observed speciation and the model of Ihinger *et al*. (1999), we calculated the apparent equilibrium temperature for each experiment (Fig. 5). The temperature was calculated to be 478 ± 19°C for runs c21, c04, p59 and p66, indicating that the cooling history is similar irrespective of experimental apparatus. On the other hand, the apparent equilibrium temperature was 1048°C for run p54. This may indicate that the H_2O speciation in run p54 was frozen at a higher temperature upon quenching because of the low H_2O content, while the other runs experienced re-equilibration at a low temperature because of a high H_2O content and thus a high reaction rate (Zhang *et al*., 2000).

Speciation of CO_2

Our result that high-SiO_2 rhyolitic glass (SiO_2 = 77.8 wt%) contains both CO_{2mol} and CO_3^{2-} appears to contrast with the general understanding that rhyolitic melt dissolves only CO_2 molecules (Fogel and Rutherford, 1990; Blank *et al*., 1993; Tamic *et al*., 2001). On the other hand, this result is consistent with Moore *et al*. (2008) who reported the presence of CO_3^{2-} in their high-SiO_2 rhyolitic melt. Here we discuss the speciation of CO_2 in the sample in detail.

In intermediate melts, CO_2 dissolves as CO_{2mol} and CO_3^{2-}:

$$CO_{2mol}\ (melt) + O^{2-}\ (melt) \leftrightarrow CO_3^{2-}\ (melt) \qquad (4)$$

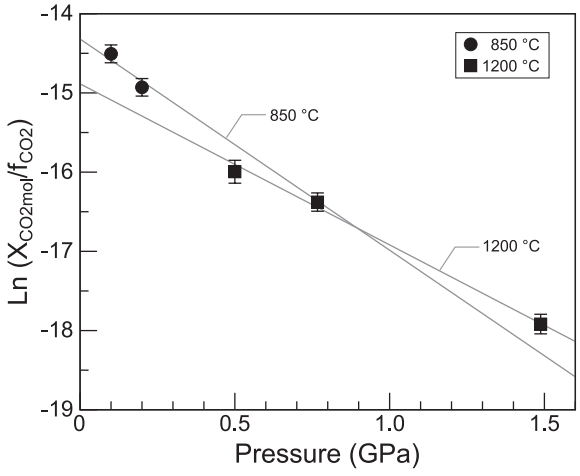

Fig. 9. Variation of $X_{CO2mol}{}^{melt}/f_{CO2}$ as a function of pressure. The symbols denote the following: ■, 1200°C experiments; ●, 850°C experiments. Lines are the best-fit isotherms at 850 and 1200°C, described by Eq. (5). CO_2 fugacity was calculated after Holloway (1977) and Flowers (1979). Parameters in Eq. (5) were calculated to be $\overline{V}^{melt}_{CO2mol}$ = 24.9 ± 2.0 cm³/mol and $\Delta_{sln}H$ = –22.2 ± 6.3 kJ/mol.

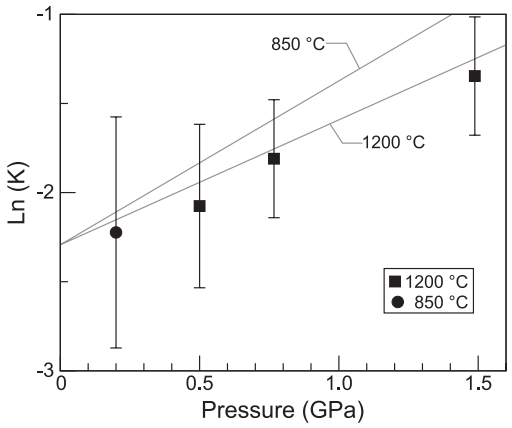

Fig. 10. Variation in equilibrium constant of reaction (6) ($K = X_{CO32-}{}^{melt}/(X_{CO2mol}{}^{melt}X_{O2-}{}^{melt})$) as a function of pressure. The symbols denote the following: ■, 1200°C experiments; ●, 850°C experiments. Lines are the best-fit isotherms at 850 and 1200°C, described by Eq. (6). Parameters were calculated to be Δ_rV = –8.6 ± 0.9 cm³/mol and Δ_rH = +1.1 ± 4.4 kJ/mol. Note that run c21 was not used in the fitting calculation and is not shown in this diagram.

where O^{2-} represents oxygen ions in the melt that are available for reaction with CO_{2mol} (non-bridging oxygen) (Blank and Brooker, 1994; Ni and Keppler, 2013). Previous studies revealed that pressure, temperature and water content affect CO_2 speciation in intermediate melts. For the pressure effect, Stolper *et al*. (1987) reported that the fraction of CO_3^{2-} increases with increasing pressure in dry albite melt. Guillot and Sator (2011) showed that, based on molecular dynamics simulation, the fraction of CO_3^{2-} is positively correlated with pressure. On the other hand, Behrens *et al*. (2004a) stated that pressure has only a minor influence on CO_2 speciation in CO_2-H_2O-dacite experiments. As for the water-content effect, the fraction of CO_3^{2-} increases with increasing H_2O content (King and Holloway, 2002; Behrens *et al*., 2004a; Botcharnikov *et al*., 2005, 2006; Duncan and Dasgupta, 2015), probably because water depolymerises the melt, thus increasing the activity of non-bridging oxygen available for CO_3^{2-} formation (King and Holloway, 2002). For the temperature effect, as temperature decreases, the fraction of CO_3^{2-} increases (Morizet *et al*., 2001; Nowak *et al*., 2003; Guillot and Sator, 2011; Konschak and Keppler, 2014).

Similar to H_2O speciation, a quenching effect is considered significant in modifying the CO_2 speciation. Because reaction (4) shifts to the right at low temperatures, the CO_3^{2-}/CO_{2mol} ratio increases during cooling until the speciation is frozen at the glass transition temperature (Morizet *et al*., 2001; Nowak *et al*., 2003). This effect is even more severe in a hydrous system, because the glass transition temperature is lowered due to the presence of water and, thus, the time available for re-equilibration is long (Duncan and Dasgupta, 2015). On the other hand, the CO_3^{2-}/CO_{2mol} ratio may decrease during quenching in a hydrous system, because the OH/H_2O_{mol} ratio decreases, and thus, the number of non-bridging oxygen (NBO) decreases. As a result of these two effects, the CO_3^{2-}/CO_{2mol} ratios may deviate from the equilibrium state at experimental temperatures, shifting to the upper-left area above the high-temperature equilibrium line in the CO_3^{2-}/CO_{2mol}-NBO/T diagram (Fig. 8). To examine this quenching effect, we analysed the CO_3^{2-}/CO_{2mol} ratios and NBO/T values for quenched glass and for high temperature melt using the model of Konschak and Keppler (2014) (Fig. 8). NBO/T values were calculated with the assumption that OH behaves as a network modifier but H_2O_{mol} does not (Zotov *et al*., 1992). Surprisingly, all of our observed data are plotted below the high temperature equilibrium line, rather than on or above the line as expected from the quenching effect. No process can explain such a downward shift. The apparent equilibrium temperature determined for H_2O speciation does not show any correlation with the observed CO_3^{2-}/CO_{2mol} ratios. One possible explanation is that the high temperature equilibrium model proposed by Konschak and Keppler (2014), which was established based on in-situ experiments on intermediate melts, cannot be used for high-SiO_2 rhyolitic melts. Rather, the equilibrium lines for high-SiO_2 rhyolite may be located far below the Konschak and Keppler model, and various degrees of CO_2 re-equilibration occurred during quenching irrespective of H_2O re-equilibration on quenching.

Currently, we cannot quantify the contribution of quenching to modifying the CO_3^{2-}/CO_{2mol} ratios. We consider that a part of CO_3^{2-} is a product of quenching, but the remaining already existed under the experimental conditions. Both pressure and water content could have contributed to the CO_3^{2-} production. Given that CO_3^{2-} has not been observed in previous experiments at lower pressure and comparable water content (Tamic *et al*., 2001), pressure is considered to be the dominant factor in stabilising CO_3^{2-} in the high-SiO_2 rhyolite.

Thermodynamics of CO_{2mol} and CO_3^{2-} speciation and solubilities for rhyolitic melt

Finally, we calculated the thermodynamic parameters related to CO_2 solubility. As discussed above, pressure may be a dominant factor in increasing the value of CO_3^{2-}/CO_{2mol} in the present experiments, although CO_2 speciation may have been modified by quenching. Here, we used our original data without any correction for the calculation.

The fluid-melt equilibrium is described by the following equation (e.g., Silver and Stolper, 1989):

$$\ln\left(\frac{X_{CO_{2mol}}^{melt}}{f_{CO_2}}\right) = \ln\left(\frac{X_{CO_{2mol}}^{melt\text{-}ref}}{f_{CO_2}^{ref}}\right) - \frac{\Delta_{sln}H}{R}\left(\frac{1}{T}-\frac{1}{T^{ref}}\right) - \frac{\overline{V}_{CO_{2mol}}^{melt}\left(P-P^{ref}\right)}{RT} \quad (5)$$

where f_{CO2} is the fugacity of CO_2, P is the total pressure, R is the gas constant, T is the temperature, X_{CO2mol}^{melt} is the molar fraction of CO_{2mol} in all the species involved in the dissolution, $\overline{V}_{CO2mol}^{melt}$ is the partial molar volume of CO_{2mol} in the melt, and $\Delta_{sln}H$ is the enthalpy of dissolution. f_{CO2} was calculated based on the model of Holloway (1977) and Flowers (1979). Fitting Eq. (5) to our data, we calculated $\overline{V}_{CO2mol}^{melt}$ and $\Delta_{sln}H$ to be 24.9 ± 2.0 cm^3/mol and –22.2 ± 6.3 kJ/mol, respectively (Fig. 9). The obtained $\overline{V}_{CO2mol}^{melt}$ is slightly lower than previously reported values of 33.04 ± 0.87 cm^3/mol (Fogel and Rutherford, 1990), 28.1 ± 1.6 cm^3/mol (Blank, 1993), and 26–32 cm^3/mol (Behrens *et al*., 2004a). This is probably due to the higher experimental pressure in our study than that in previous studies. The $\Delta_{sln}H$ value we obtained was similar to the previously published values of –20.32 ± 3.18 kJ/mol (Fogel and Rutherford, 1990) and –27.1 ± 2.0 kJ/mol (Blank, 1993). The negative enthalpy means that dissolution occurs exothermally and is consistent with the recent understanding that CO_2 solubility is negatively correlated with temperature (e.g., Ni and Keppler, 2013).

Next, we analysed the speciation reaction (4) (Fig. 10). Fitting the following equation to the data,

$$\ln\frac{K}{K^{ref}} = -\frac{\Delta_r V}{RT}\left(P-P^{ref}\right) - \frac{\Delta_r H}{R}\left(\frac{1}{T}-\frac{1}{T^{ref}}\right) \quad (6)$$

we obtained the changes in the partial molar volume of CO_2, $\Delta_r V$, as –8.6 ± 0.9 cm^3/mol and reaction enthalpy, $\Delta_r H$, as +1.1 ± 4.4 kJ/mol. This value of $\Delta_r V$ was of the same order of magnitude as that of albite melt (–3.9 ± 0.8 cm^3/mol; Stolper *et al*., 1987). $\Delta_r H$ is accompanied by a large error, mainly owing to limited experimental data. Additional experiments over a wider range of temperatures are necessary to improve our understanding of the CO_2-H_2O solubility in high-SiO_2 rhyolitic systems.

Summary

Fluid saturation experiments in a rhyolitic melt-CO_2-H_2O system at 850 and 1200°C and 0.1–1.5 GPa, together with infrared spectroscopy of the quenched glass, showed that both CO_2 molecules (CO_{2mol}) and carbonate anions (CO_3^{2-}) were present in the high-SiO_2 rhyolitic glass. The concentrations were 199–9188 ppm and 58–2123 ppm for CO_{2mol} and CO_3^{2-}, respectively. The extinction coefficients for CO_{2mol} and CO_3^{2-} were newly determined to be ε_{2350} = 1192 ± 130 L·cm^{-1}·mol^{-1} (CO_{2mol}) and ε_{1410} = 91 ± 28 L·cm^{-1}·mol^{-1} (CO_3^{2-}). The total H_2O content was 2.6–6.1 wt%. The speciation observed in quenched glasses may reflect both the original speciation at high temperatures and modification due to quenching. Using our original data obtained from quenched glass samples, we calculated the partial molar volume of CO_{2mol} and dissolution enthalpy to be $\overline{V}_{CO2mol}^{melt}$ = 24.9 ± 2.0 cm^3/mol and $\Delta_{sln}H$ = –22.2 ± 6.3 kJ/mol, respectively. The changes of volume and enthalpy upon the formation reaction of CO_3^{2-} were calculated to be $\Delta_r V$ = –8.6 ± 0.9 cm^3/mol and $\Delta_r H$ = +1.1 ± 4.4 kJ/mol, respectively.

Acknowledgments—We are grateful to Edward M. Stolper and his assistant Janice Grancich for providing PhD thesis of Jennifer G. Blank (Blank, 1993). We thank Takahiro Watanabe for helpful advices on vacuum extraction analysis. Infrared spectroscopy was carried out at the Open Facility, CRIS, Hokkaido University. Comments by Richard Brooker were helpful to improve the earlier version of the manuscript. Official reviews by Penny King and Roman Botcharnikov significantly improved the manuscript. Editor Tetsu Kogiso gave us helpful comments and encouragement. This study was partly supported by JSPS Research Fellowships for Young Scientists and Grant-in-Aid for Research Activity Start-up to Yoshimura and MEXT Grant-in-Aid for Scientific Research to Nakamura and to Yurimoto.

References

Anderson, A. T., Davis, A. M. and Lu, F. (2000) Evolution of Bishop Tuff rhyolitic magma based on melt and magnetite inclusions and zoned phenocrysts. *J. Petrol*. **41**, 449–473.

Bachmann, O., Wallace, P. J. and Bourquin, J. (2009) The melt inclusion record from the rhyolitic Kos Plateau Tuff (Aegean Arc). *Contrib. Mineral. Petrol*. **159**, 187–202.

Behrens, H., Ohlhorst, S., Holtz, F. and Champenios, M. (2004a) CO_2 solubility in dacitic melts equilibrated with H_2O-CO_2 fluids: Implications for modeling the solubility of CO_2 in silicic melts. *Geochim. Cosmochim. Acta* **68**, 4687–4703.

Behrens, H., Tamic, N. and Holtz, F. (2004b) Determination of the molar absorption coefficient for the infrared absorption band of CO_2 in rhyolitic glasses. *Am. Mineral*. **89**, 301–306.

Blank, J. G. (1993) An experimental investigation of the behavior of carbon dioxide in rhyolitic melt. Ph.D. Diss., California Institute of Technology.

Blank, J. G. and Brooker, R. A. (1994) Experimental studies of carbon dioxide in silicate melts: solubility, speciation, and stable carbon isotope behavior. *Reviews in Mineralogy and Geochemistry* **30** (Carroll, M. R. and Holloway, J. R., eds.), 157–186, Mineralogical Society of America.

Blank, J. G., Stolper, E. M. and Carroll, M. R. (1993) Solubilities of carbon dioxide and water in rhyolitic melt at 850°C and 750 bars. *Earth Planet. Sci. Lett*. **119**, 27–36.

Blundy, J., Cashman, K. V., Rust, A. and Witham, F. (2010) A case for CO_2-rich arc magmas. *Earth Planet. Sci. Lett*. **290**, 289–301.

Botcharnikov, R., Freise, M., Holtz, F. and Behrens, H. (2005) Solubility of C-O-H mixtures in natural melts: new experimental data and application range of recent models. *Ann. Geophys*. **48**, 633–646.

Botcharnikov, R., Behrens, H. and Holtz, F. (2006) Solubility and speciation of C-O-H fluids in andesitic melt at T=1100–1300°C and P=200 and 500MPa. *Chem. Geol*. **229**, 125–143.

Brenan, J. M. and Watson, E. B. (1988) Fluids in the lithosphere, 2. Experimental constraints on CO_2 transport in dunite and quartzite at elevated P-T conditions with implications for mantle and crustal decarbonation processes. *Earth Planet. Sci. Lett*. **91**, 141–158.

Brey, G. (1976) CO_2 solubility and solubility mechanisms in silicate melts at high pressures. *Contrib. Mineral. Petrol*. **57**, 215–221.

Brooker, R. A., Kohn, S. C., Holloway, J. R., McMillan, P. F. and Carroll, M. R. (1999) Solubility, speciation and dissolution mechanisms for CO_2 in melts on the $NaAlO_2$-SiO_2 join. *Geochim. Cosmochim. Acta* **63**, 3549–3565.

Duan, X. (2014) A general model for predicting the solubility behavior of H_2O-CO_2 fluids in silicate melts over a wide range of pressure, temperature and compositions. *Geochim. Cosmochim. Acta* **125**, 582–609.

Duncan, M. S. and Dasgupta, R. (2014) CO_2 solubility and speciation in rhyolitic sediment partial melts at 1.5–3.0 GPa—Implications for carbon flux in subduction zones. *Geochim. Cosmochim. Acta* **124**, 328–347.

Duncan, M. S. and Dasgupta, R. (2015) Pressure and temperature dependence of CO_2 solubility in hydrous rhyolitic melt: implications for carbon transfer to mantle source of volcanic arcs via partial melt of subducting crustal lithologies. *Contrib. Mineral. Petrol*. **169**, 54.

Fine, G. and Stolper, E. (1985) The speciation of carbon dioxide in sodium aluminosilicate glasses. *Contrib. Mineral. Petrol*. **91**, 105–121.

Flowers, G. C. (1979) Correction of Holloway's (1977) Adaptation of the modified Redlich-Kwong equation of state for calculation of the fugacities of molecular species in supercritical fluids of geologic interest. *Contrib. Mineral. Petrol*. **69**, 315–318.

Fogel, R. A. and Rutherford, M. J. (1990) The solubility of carbon dioxide in rhyolitic melts: A quantitative FTIR study. *Am. Mineral*. **75**, 1311–1326.

Ghiorso, M. S. and Gualda, G. A. R. (2015) An H_2O-CO_2 mixed fluid saturation model compatible with rhyolite-MELTS. *Contrib. Mineral. Petrol*. **169**, 53.

Gordon, S. and McBride, B. J. (1996) Computer program for calculation of complex chemical equilibrium compositions and applications II. Users manual and program description: NASA Ref. Pub., vol. 1311

Guillot, B. and Sator, N. (2011) Carbon dioxide in silicate melts: A molecular dynamics simulation study. *Geochim. Cosmochim. Acta* **75**, 1829–1857.

Harris, D. M. and Rose, W. I. (1996) Dynamics of carbon dioxide emissions, crystallization, and magma ascent: hypotheses, theory, and applications to volcano monitoring at Mount St. Helens. *Bull. Volcanol*. **58**, 163–174.

Harris, D. M., Sato, M., Casadevall, T. J., Rose, W. I. and Bornhorst, T. J. (1981) Emission rates of CO_2 from plume measurements. *US Geol. Surv. Prof. Paper* **1250**, 201–207.

Holloway, J. R. (1977) Fugacity and activity of molecular species in supercritical fluids. *Thermodynamics in Geology* (Fraser, D. G., ed.), 161–181, D. Reidel.

Ihinger, P. D., Hervig, R. L. and McMillan, P. F. (1994) Analytical methods for volcatiles in glasses. *Reviews in Mineralogy and Geochemistry* **30** (Carroll, M. R. and Holloway, J. R., eds.), 67–121, Mineralogical Society of America.

Ihinger, P. D., Zhang, Y. and Stolper, E. M. (1999) The speciation of dissolved water in rhyolitic melt. *Geochim. Cosmochim. Acta* **63**, 3567–3578.

King, P. L. and Holloway, J. R. (2002) CO_2 solubility and speciation in intermediate (andesitic) melts: The role of H_2O and composition. *Geochim. Cosmochim. Acta* **66**, 1627–1640.

Kingery, W. D. and Berg, M. (1955) Study of the initial stages of sintering solids by viscous flow, evaporation-condensation, and self-diffusion. *J. Appl. Phys*. **26**, 1205–1212.

Konschak, A. and Keppler, H. (2014) The speciation of carbon dioxide in silicate melts. *Contrib. Mineral. Petrol*. **167**, 998.

Liu, Y., Zhang, Y. and Behrens, H. (2005) Solubility of H_2O in rhyolitic melts at low pressures and new empirical model for mixed H_2O-CO_2 solubility in rhyolitic melts. *J. Volcanol. Geotherm. Res*. **143**, 219–235.

Lupulescu, A. and Watson, E. B. (1999) Low melt fraction connectivity of granitic and tonalitic melts in a mafic crustal rock at 800°C and 1 GPa. *Contrib. Mineral. Petrol*. **134**, 202–216.

Moore, G., Roggensack, K. and Klonowski, S. (2008) A low-pressure-high-temperature technique for the piston-cylinder. *Am. Mineral*. **93**, 48–52.

Morizet, Y., Kohn, S. C. and Brooker, R. A. (2001) Annealing experiments on CO_2-bearing jadeite glass: an insight into the true temperature dependence of CO_2 speciation in silicate melts. *Mineral. Mag*. **65**, 701–707.

Morizet, Y., Brooker, R. A. and Kohn, S. C. (2002) CO_2 in haplophonolite melt: solubility, speciation and carbonate complexation. *Geochim. Cosmochim. Acta* **66**, 1809–1820.

Mysen, B. O. (1976) The role of volatiles in silicate melts: solubility of carbon dioxide and water in feldspar, pyroxene, and feldsparthoid melts to 30 kb and 1625°C. *Am. J. Sci*. **276**, 969–996.

Mysen, B. O., Arculus, R. J. and Eggler, D. H. (1975) Solubility of carbon dioxide in melts of andesite, tholeiite, and olivine nephelinite composition to 3 GPa pressure. *Contrib. Mineral. Petrol*. **53**, 227–239.

Nakamura, M. and Watson, E. B. (2001) Experimental study of aqueous fluid infiltration into quartzite: implications for the kinetics of fluid redistribution and grain growth driven by interfacial energy reduction. *Geofluids* **1**, 73–89.

Ni, H. and Keppler, H. (2013) Carbon in silicate melts. *Reviews in Mineralogy and Geochemistry* **75** (Hanzen, R. M., Jones, A. P. and Baross, J. A., eds.), 251–287, Mineralogical Society of America.

Nowak, M., Porbatzki, D., Spickenbom, K. and Diedrich, O. (2003) Carbon dioxide speciation in silicate melts: a restart. *Earth Planet. Sci. Lett*. **207**, 131–139.

Nowak, M., Schreen, D. and Spickenbom, K. (2004) Argon and CO_2 on the race track in silicate melts: A tool for the development of a CO_2 speciation and diffusion model. *Geochim. Cosmochim. Acta* **68**, 5127–5138.

Okumura, S. and Nakashima, S. (2005) Molar absorptivities of OH and H_2O in rhyolitic glass at room temperature and at 400–600°C. *Am. Mineral*. **90**, 441–447.

Papale, P., Moretti, R. and Barbato, D. (2006) The compositional dependence of the saturation surface of H_2O+CO_2 fluids in silicate melts. *Chem. Geol*., **229**, 78–45.

Rust, A. C., Cashman, K. V. and Wallace, P. J. (2004) Magma degassing buffered by vapor flow through brecciated conduit margins. *Geology* **32**, 349–352.

Silver, L. and Stolper, E. (1989) Water in albitic glasses. *J. Petrol*. **30**, 667–709.

Stolper, E., Fine, G., Johnson, H. and Newman, S. (1987) Solubility of carbon dioxide in albitic melt. *Am. Mineral*. **72**, 1071–1085.

Tamic, N., Behrens, H. and Holtz, F. (2001) The solubility of H_2O and CO_2 in rhyolitic melts in equilibrium with a mixed CO_2-H_2O fluid phase. *Chem. Geol*. **174**, 333–347.

Wallace, P. J., Anderson, A. T. and Davis, A. M. (1999) Gradients in H_2O, CO_2, and exsolved gas in a large-volume silicic magma systems: Interpreting the record preserved in melt inclusions from the Bishop Tuff. *J. Geophys. Res*. **104**, 20097–20122.

Watson, E. B. and Lupulescu, A. (1993) Aqueous fluid connectivity and chemical transport in clinopyroxene-rich rocks. *Earth Planet. Sci. Lett*. **117**, 279–294.

Yoshimura, S. and Nakamura, M. (2010) Chemically driven growth and resorption of bubbles in a multivolatile magmatic system. *Chem. Geol*. **276**, 18–28.

Zhang, Y. (1999) H_2O in rhyolitic glasses and melts: measurement, speciation, solubility, and diffusion. *Rev. Geophys*. **37**, 439–516.

Zhang, Y., Xu, Z. and Behrens, H. (2000) Hydrous species geospeedmeter in rhyolite: Improved calibration and application. *Geochim. Cosmochim. Acta* **64**, 3347–3355.

Zotov, N., Yanev, Y., Epelbaum, M. and Konstantinov, L. (1992) Effect of water on the structure of rhyolite glass—X-ray diffraction and Raman spectroscopy studies. *J. Non-Cryst. Solids* **142**, 234–246.

Supplementary Materials

URL (http://www.terrapub.co.jp/journals/GJ/archives/data/51/MS466.pdf)
Table S1